Liquid metal extraction of Nd from NdFeB magnet scrap

Y. Xu, L.S. Chumbley, and F.C. Laabs
Ames Laboratory and the Materials Science & Engineering Department, Iowa State University, Ames, Iowa 50011

(Received 23 February 2000; accepted 16 June 2000)

This research involves using molten magnesium (Mg) to remove neodymium (Nd) from NdFeB magnet scrap by diffusion. Mg was melted over pieces of NdFeB scrap and held at temperatures in the range 675–705 °C for 2–8 h. The Mg was allowed to solidify, and the castings were then sectioned and characterized using scanning electron microscopy, x-ray diffraction, and chemical analysis. Nd was found to have diffused out of the solid scrap into the molten Mg. The thickness of the diffusion layer was measured, the diffusion of Nd through the NdFeB scrap into liquid Mg was described, and the diffusion coefficient of Nd in liquid Mg was estimated.

I. INTRODUCTION

In recent years NdFeB-based magnet materials have emerged as the leaders in high-field permanent magnet applications. They exhibit the highest energy product of all permanent magnets and possess excellent resistance to demagnetization at normal operating temperatures. NdFeB magnets have become widely used in automotive cranking motors, computers, audio-visual components, magnetic separators, military and aerospace systems, and other devices that require high-field magnets of reduced size and weight.

During this last decade, the United States Bureau of Mines investigated several processing techniques for recovery of valuable rare-earth elements from NdFeB magnet scrap. The best separation of rare-earth from NdFeB magnet scrap obtained by Morrison[1] and Lyman and Palmer[2] was using sulfuric acid to dissolve the scrap, followed by precipitation of sodium and ammonium intermediate double salts, and then converting those rare-earth salts to useful neodymium product NdF_3 by using HF. In 1993, Greenberg[3] obtained neodymium trifluoride from NdFeB swarf (a mixture of oil, machining chips, and other solid residue) and slag by using hydrofluoric acid. As in Ref. 1, this method involved a number of chemical extraction and reduction steps, and both methods require the use of large amounts of dangerous solutions. Due to the complexity and expense of returning to an oxide or fluoride state these methodologies are impractical for recycling purposes.[5] With the current expansion of the NdFeB magnet market, more and more scrap is being stockpiled due to the lack of a cost-efficient recycling method.[1] It is clear that development of a viable method to recycle NdFeB scrap is desirable for economic and environmental reasons.[5]

This study focused on liquid metal extraction processing to recycle Nd from NdFeB scrap. Researchers at Ames Laboratory are pioneers in this area, applying the general method to a number of systems.[4,5] In this study liquid Mg was used as the extractant to remove Nd from magnet scrap. Nd is soluble in liquid Mg and forms a number of intermetallic compounds while Fe and B are essentially immiscible in Mg. Therefore, liquid Mg readily accepts Nd, forming a Mg–Nd solution, while leaving the Fe and B behind.

The production of a Nd-rich alloy should find application in the Mg casting industry, where rare earths are routinely added to improve mechanical properties. Magnesium alloys with rare-earth elements (e.g., neodymium, yttrium) together with zirconium exhibit improved creep resistance at elevated temperatures, reduced microporosity in castings, and improved weldability.[6] Currently the price of such castings is very expensive. For example, in a typical casting of QE22 containing only 2.2 wt% Nd, the cost of the Nd accounts for over 40% of the cost of raw materials.[7] These costs can be lowered if a master Mg–Nd alloy can be produced by an inexpensive recycling scheme. Thus, a successful extraction of Nd into Mg in a useable form will eliminate wastes and lower subsequent alloy casting costs as well.

II. EXPERIMENTAL PROCEDURE

The starting material for all experiments consisted of irregularly shaped pieces of magnet scrap produced by powder processing. The average composition of the scrap as determined by chemical analysis of test samples is shown in Table I.

The purity of magnesium used was 99.8% (metal basis). The NdFeB scrap was placed in a 5 cm diameter ×10 cm high stainless steel crucible along with pieces of

pure Mg. The general geometry and size of the pieces is shown in Fig. 1. The size of scrap is larger than 10 mesh. The crucibles were then induction heated using a 25 kW, 3000 Hz Lepel generator in an atmosphere controlled chamber to temperatures ranging from 675 to 750 °C for times ranging from 2 to 8 h. The temperature was measured continuously by a Pt–13% Rh thermal couple. Before heating, the chamber was evacuated then back-filled with Ar whose purity is greater than 99% to maintain a clean environment and minimize oxidation and vaporization of the Mg.

After being held at the predetermined temperature for the specified time, the crucibles were cooled and the molten Mg was allowed to solidify in the crucible. The crucibles were then cross-sectioned and polished for analysis. Characterization of the cast samples was carried out using a scanning electron microscopy (SEM) equipped with energy dispersive spectrosocopy (EDS), x-ray diffraction (XRD), and chemical analysis using inductively coupled plasma (ICP).

III. EXPERIMENTAL RESULT

A. Microstructure of the NdFeB scrap and diffusion region

A typical cast sample is shown in Fig. 2. The constituents of the casting, namely the now solidified Mg and the scrap NdFeB pieces, are clearly seen in Figs. 2(a) and 2(b). Figure 3 is a series of high magnification micrographs showing the phases present in the various regions as you transition from the unaffected NdFeB/diffusion layer to the diffusion layer/solidified Mg interface.

Close observation of the sample using backscattered electron imaging (BSE) reveals that the scrap consists of three distinct phases. The compositions of these phases are shown in Table II. Note that due to the difficulty of using EDS to quantitatively determine B (which is only present in small amounts) this element is not listed. The identifications made in Table II are based on the relative amounts of Nd and Fe detected, and the phases known to commonly exist in Fe–Nd–B magnet materials.[8–10] Upon this basis, the light gray phase that constitutes the matrix

TABLE I. Overall composition of NdFeB scrap. Nd, Fe, B, Pr, and Dy are given in weight percent, and C, N, and O are given in parts per million.

Nd	Fe	B	Pr	Dy	C	N	O
(±1.0)	(±0.7)	(±0.04)	(±0.01)	(±0.3)			
18.0	72.4	0.90	1.82	5.3	0.0336	29	343

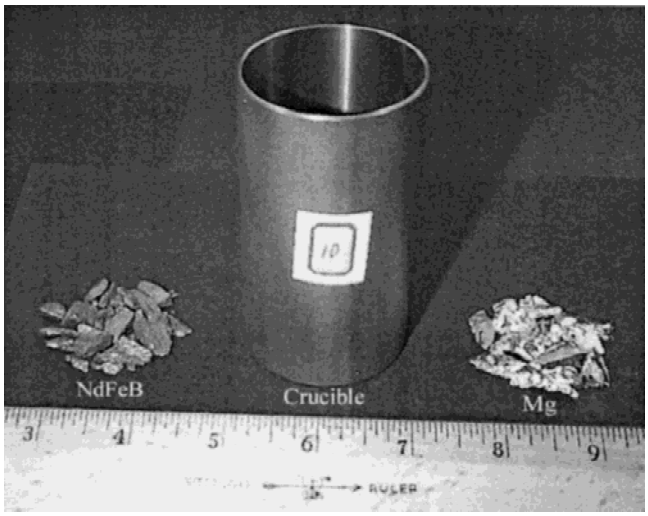

FIG. 1. Geometry of NdFeB scrap, stainless steel crucible, and pure Mg.

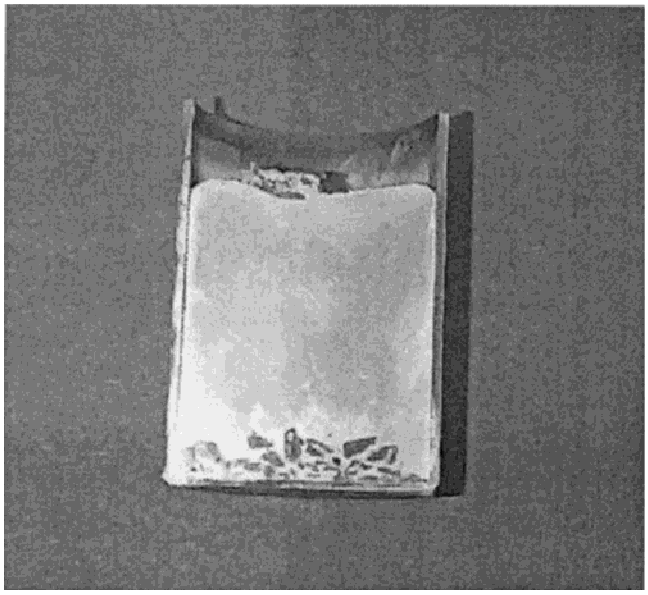

(a)

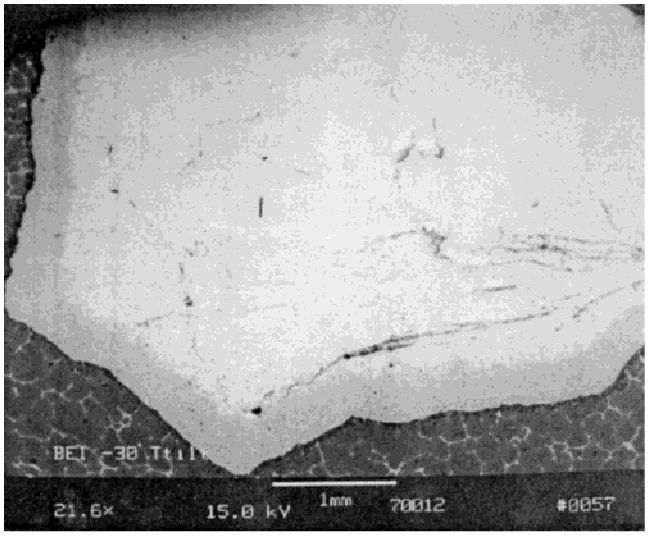

(b)

FIG. 2. (a) Macrostructure and (b) microstructure of the cast sample.

of the magnet material and marked as "1" in Fig. 3(a) is identified as $Nd_2Fe_{14}B$, while the medium gray phase is Nd_2Fe_{17}. The third phase ["3" in Fig. 3(a)] only has minor amounts of Nd and is identified as α–Fe with some Nd in solid solution. In the transition region shown in Fig. 3(b) a Nd-depleted region exists where diffusion of the Nd from the scrap has occurred. The same phases are observed in this region, namely, $Nd_2Fe_{14}B$, Nd_2Fe_{17}, and α–Fe + Nd, although now α–Fe + Nd is the dominant phase in the diffusion layer. The diffusion layer/solidified Mg interface is shown in Fig. 3(c). The major phase is again α–Fe + Nd. Near the interface but within the α–Fe + Nd diffusion zone a few small white particles can be seen. These particles are identified as $NdFe_4B_4$. The composition changes abruptly at the interface as the now solidified Mg becomes the matrix phase. Although

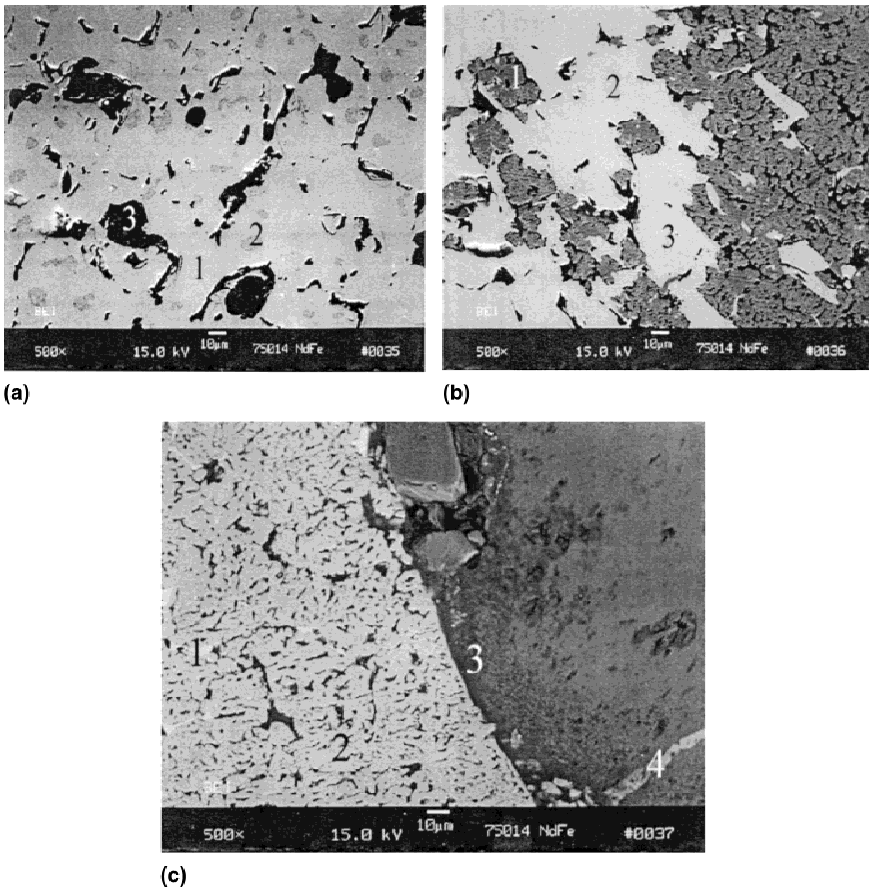

FIG. 3. Micrographs showing the various regions from unaffected NdFeB scrap to solidified Mg: (a) unaffected scrap NdFeB, (b) interface between unaffected and diffusion depleted zone in solid scrap, and (c) interface between diffusion depleted zone and solidified Mg + Nd.

TABLE II. The EDS results and phase analysis. The asterisked data indicate questionable data.

		Composition (wt%)				
Fig. 3 Micrograph		Nd ±0.40	Fe ±0.35	Mg ±0.50	Phase	Description
(a) NdFeB	Spot 1	22.48	77.52	⋯	$Nd_2Fe_{14}B$	Light gray
	Spot 2	17.82	82.18	⋯	Nd_2Fe_{17}	Medium gray
	Spot 3	0.73	99.27	⋯	α–Fe + Nd	Dark gray
(b) Scrap/diffusion layer	Spot 1	0.33*	99.67	⋯	α–Fe + Nd	Dark gray
	Spot 2	17.90	82.10	⋯	Nd_2Fe_{17}	Medium gray
	Spot 3	21.45	78.55	⋯	$Nd_2Fe_{14}B$	Light gray
(c) Diffusion layer/solidified mg	Spot 1	36.34	63.66	⋯	$NdFe_4B_4$	White
	Spot 2	0.45*	99.55	⋯	α–Fe + Nd	Medium gray
	Spot 3	2.1	1.9	95.8	Mg + Nd	Dark gray
	Spot 4	34.92	0.28*	64.8	$Mg_{12}Nd$	Light gray

Mg and Fe are essentially immiscible, right at the interface a small amount of Fe was detected, along with Nd in solid solution. However, the low values detected are less than one standard deviation away from the measured mean. Therefore, statistically they are considered nondefinitive and are subject to question.

B. Microstructure of the solidified magnesium matrix

The microstructure of the solidified Mg consists of grains of Mg with a Nd-rich intermetallic phase present at the grain boundaries, Fig. 4(a). Within the grains a fine platelike Widmanstatten structure is observed, Fig. 4(b). X-ray EDS analysis revealed that the matrix contains Nd present in solid solution in amounts up to 2.0 wt%. The phase distributed on the grain boundaries contains ≈ 32–36 wt% of Nd (e.g. spot 4, Table II) and is identified as $Mg_{12}Nd$. Although the needles are too small for accurate EDS analysis, being less than 0.1 μm in thickness, the Mg–Nd phase diagram predicts that upon cooling $Mg_{12}Nd$ will precipitate from a supersaturated solid solution. This agrees with BSE observations since they possess the same contrast level as the intergranular $Mg_{12}Nd$ easily identified using EDS.

XRD scans of the matrix were run to confirm this identification. A typical spectra obtained from the matrix is shown in Fig. 5 with a listing of the observed peaks shown in Table III. All of the peaks in the XRD scans could be identified as either Mg or $Mg_{12}Nd$.

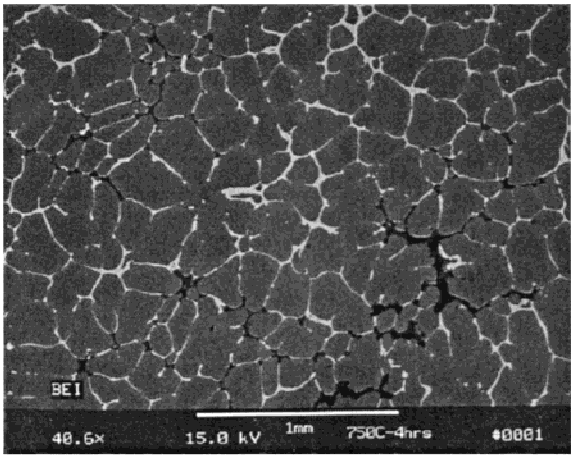

(a)

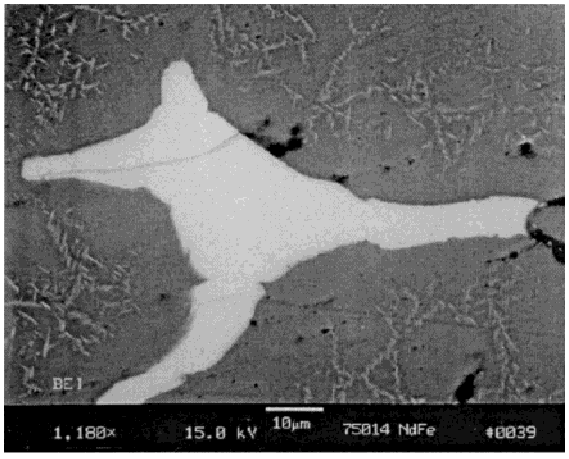

(b)

FIG. 4. Microstructure of molten Mg in the cast condition: (a) Overall appearance of the matrix and (b) close-up showing the intergranular phase and Widmanstatten structure.

IV. DISCUSSION

The phase diagram for Mg–Nd is shown in Fig. 6.[11] While numerous Mg–Nd phases have been identified, the exact nature of the phase diagram is still unknown. From observation of the microstructure it appears that the high affinity of Mg for Nd causes Nd to rapidly diffuse out of the solid NdFeB scrap and into the liquid Mg at high temperatures. While the amount of Nd present in the matrix depends on hold time and temperature and varies for each casting, chemical analysis of the once molten Mg matrices shows that on average the total Nd content falls to near the solubility limit of Nd in Mg. Upon solidification, Mg grains nucleate and grow, becoming enriched in Nd as solidification proceeds. At the eutectic temperature the composition of the remaining liquid approaches that of the intermetallic $Mg_{12}Nd$. This phase nucleates and grows on the grain boundaries upon solidification. As the Nd-supersaturated Mg matrix cools, the intermetallic also nucleates and precipitates within the Mg grains in the form of a Widmanstatten structure.

A. Diffusion of Nd through NdFeB scrap

The thickness of the diffusion layer was determined by making a number of measurements on SEM micrographs and averaging the results. Because the scrap particulate was of irregular size and shape and spaced randomly within the crucibles, differences in sectioning of the particles during polishing is expected. Any section not made per-

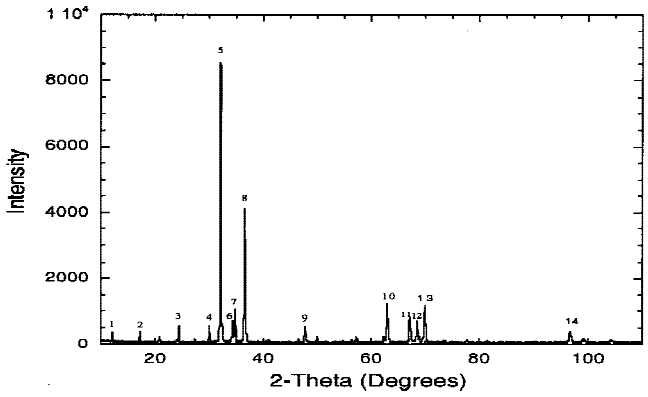

FIG. 5. X-ray diffraction scan of solidified Mg + Nd.

pendicular to the diffusion direction will result in the diffusion zone appearing wider than what actually exists. To minimize this effect, measurements were obtained only from large particulate where the diffusion zone appeared of relatively constant thickness around the diameter, the assumption being that these zones most closely approach the actual width of the diffusion layer. This method assures that, at worst, the measured diffusion layer thickness will be slightly overestimated. Figure 7 shows a plot of the mean diffusion layer thickness at 700, 725, and 750 °C. Since only one sample was cast at 675 °C, it is not shown in this figure.

An automated EDS line scan was run beginning in the unaffected NdFeB scrap, through the diffusion layer, and into the Mg matrix for the sample cast at 725 °C for 8 h. The total length of the line scan was 1500 μm, with the composition being sampled every 3.75 μm for a total number of 400 steps. The spectra were acquired for 200 s and the data analyzed using a standards analysis. The composition profile is shown in Fig. 8. There are two important things that must be noted. First, the compositions listed in this figure are based solely on a measurement of the Fe, Nd, and Mg x-rays collected from the sample. B could not be detected reliably, and the Pr and Dy known to be in the sample were ignored for this study. This causes the measured composition of Nd in the scrap, when normalized to one, to be closer to 27.0 wt% than the overall composition of 18.0 wt% determined by ICP. Second, there are many high-Nd points in Fig. 8. These points originate from the high Nd content phases identified optically that are distributed throughout the NdFeB scrap, the diffusion zone, and the solidified Mg. For example, in the diffusion zone small remnant regions of the starting material are seen as is the intermetallic phase Nd_2Fe_{17}. In the Mg matrix the interme tallic $Mg_{12}Nd$ can be seen optically both interden-

TABLE III. Indices of each x-ray peak.

Peak no.	2θ	Mg (*hkl*)	$Mg_{12}Nd$ (*hkl*)
1	12.0968		110
2	17.1809		101
3	24.3965		211
4	30.0117		301
5	32.0223	100	
6	34.3376	002	
7	34.7538		202
8	36.5487	101	
9	47.7672	102	
10	63.0056	103	
11	67.0932	200	
12	68.5282	112	224
13	69.8362	201	314
14	96.6355	211	

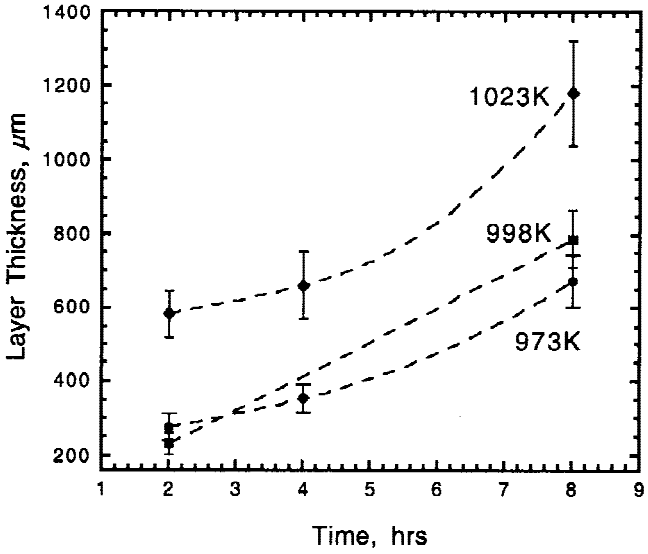

FIG. 7. Diffusion layer thickness as determined from SEM micrographs at 973 K (700 °C), 998 K (725 °C), and 1023 K (750 °C).

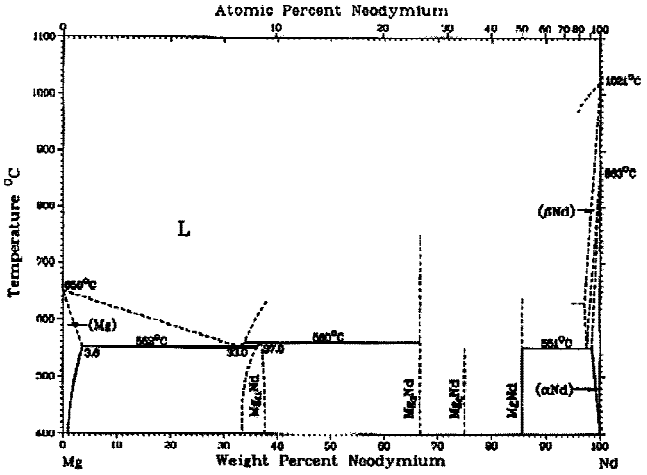

FIG. 6. Mg–Nd phase diagram.

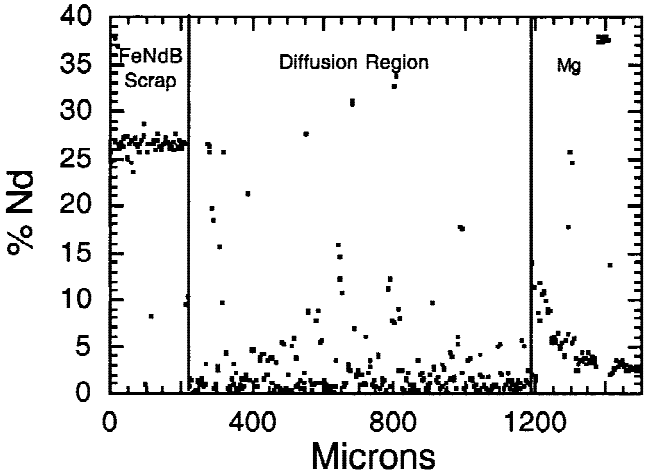

FIG. 8. Composition profile for Nd across the diffusion layer.

dritically and as part of the Widmanstatten structure. These regions cause outlying points in the EDS data as the line scan crosses them. If one ignores these points, curves can be fit to the three distinct regions comprised by the NdFeB scrap, the diffusion layer, and the Mg matrix. These are shown in Fig. 9. Note that for the diffusion region, the points having Nd content >5 wt% were ignored since these were observed to be intermetallic compounds. Similarly, the points having Nd content higher or lower than 27 wt% were ignored in the unaffected scrap for the same reason. The scrap and diffusion zone regions exhibit linear curve fits while the solidified Mg fits well to a logarithmic curve. From these data the average composition of Nd in the scrap (excluding the contribution of Pr, Dy, and B) is ≈ 27.4 wt% Nd. The diffusion region is remarkably low in Nd, being ≈ 1.0 wt%. In order to account for the presence of the Pr, Dy, and B, a simple ratio comparing the wt % Nd in the EDS scans to the more accurate value determined by ICP can be made. When this is done the wt% Nd in the diffusion region falls to 0.67 wt%.

Using the Nd concentration profile across the diffusion layer obtained from the EDS line scan, the mass transport in the system can be described by making two assumptions. These are the following.

Assumption 1: The sold/liquid interface does not move and the average composition in the depleted scrap zone remains constant. Call this composition C_Z.

Assumption 1 is reasonable since observation of the Fe–Mg phase diagram shows that there is extremely low solubility of Fe in Mg and the two are essentially immiscible. Little or no Fe will diffuse into the liquid Mg. Thus, the Fe present in the scrap material remains as a matrix through which the Nd is diffusing and the solid/liquid interface remains fixed at the position it had at the start of the experiment. The composition of the Nd in the Fe matrix (as determined by EDS data) remains relatively constant.

Assumption 2: The thickness of the Nd enriched boundary layer in liquid Mg at the interface remains constant during the casting process. Call this thickness δ. Outside this boundary layer the liquid Mg has a uniform composition which will rise during the casting process. Call this composition C_l.

Assumption 2 is also reasonable since significant convection occurs in the liquid Mg during the casting process. The sources of convection include the thermal convection due to the horizontal temperature gradients inherent in a crucible heated from the sides and solute convection due to the horizontal composition gradient. The degree of convection should remain relatively constant during the process, ensuring that the boundary layer δ remains fairly constant. As the liquid Mg becomes enriched in Nd, convection causes the overall composition of the liquid to rise uniformly.

The diffusion process is schematically shown in Fig. 10. As the Nd diffuses into the liquid at time t_0, a two-phase zone, containing very little Nd, is generated at the interface. While two-phase zones do not occur in binary systems, this system can be thought of as a ternary between the magnet scrap, the magnesium, and the

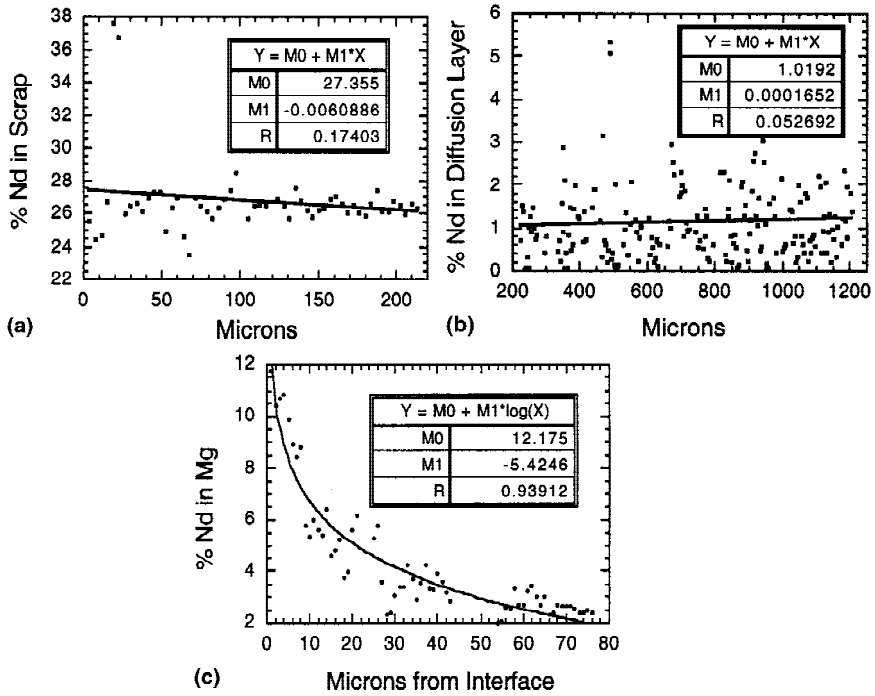

FIG. 9. Fitted curves for Nd concentration profile for the three regions across the diffusion layer.

Fe-rich diffusion zone. Thus, a two-phase region can form. Let the composition in this zone be designated C_Z. The driving force for the diffusion of the Nd through the two-phase zone is the chemical potential gradient of Nd. Most of the Nd in the two-phase zone must be tied up as a compound with Fe (Nd_2Fe_{17}). In fact, small compounds are seen optically and can be identified in the EDS line scan. Simultaneous with the formation of the two-phase region is an enrichment of the liquid at the interface in Nd. As diffusion proceeds (t_1), the overall composition of Nd in the diffusion zone remains at C_Z while the liquid at the liquid/solid interface continues to become enriched in Nd. This enrichment reaches a limiting value (C_i) and thickness (δ) as determined by the convection in the liquid. The overall composition of Nd in the liquid also starts to rise, convection also assuring that the composition remains fairly constant throughout the liquid at C_l. This composition will rise uniformly throughout the liquid. As the process continues (t_2) C_Z, remains constant while the width of the two-phase region L increases.

The Nd flux out of the scrap (F_1) and the Nd flux into the liquid Mg (F_2) must be equal because all of the mass of Nd being removed from the NdFeB scrap ends up in the liquid Mg, i.e., $F_1 = F_2$. The values for F_1 and F_2 can be written as[12,13]

$$F_1 = (C_s - C_z)\frac{dL}{dt} \quad , \tag{1}$$

$$F_2 = D\left(\frac{dC}{dZ}\right)_i \approx (D_0\, e^{-Q1RT})\frac{C_i}{\delta} \quad , \tag{2}$$

$$F_1 = F_2 \quad , \tag{3}$$

where F_1 is the flux out of the NdFeB scrap into the two-phase zone, F_2 the flux out of the two-phase zone into the liquid Mg, C_S the average composition of Nd in the two-phase zone, L the average thickness of the diffusion zone, t holding time at temperature T, D the temperature dependent diffusion coefficient of Nd in liquid Mg, D_0 temperature independent constant, known as the frequency factor, Q the activation energy, R 8.3143 J/(K mol), C the composition of Nd in liquid Mg at the solid/liquid interface, and δ the thickness of the boundary layer in liquid Mg at the solid/liquid interface.

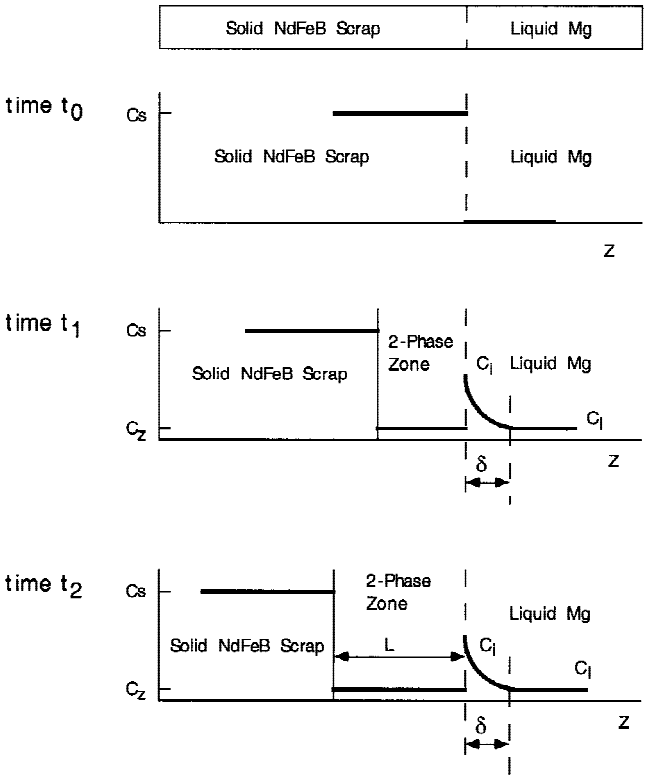

FIG. 10. Schema indicating the mass transport process of the Nd from NdFeB scrap to liquid Mg. A two-phase zone is formed in this process.

B. Estimates of the diffusion coefficient of Nd in liquid magnesium, *D*

Values for the parameters (C_S, C_Z, C_i, and δ) in Eqs. (1) and (2) can be determined by comparison of Figure 9 with the experimentally determined values from the EDS scan. The values of these parameters are shown in Table IV. Note that the adjusted Nd composition values which take the contribution of Pr, Dy, and B into account are based on the scrap having an initial Nd composition around 18.0 wt%. These values can be used to

TABLE IV. Parameters in Eqs. (1) and (2) determined by Fig. 9.

	Nd composition			
	C_s (wt%)	C_z (wt%)	C_i (wt%)	Thickness of boundary layer δ (μm)
Measured values	27.36	1.02	12.18	74.0
Adjusted values	18.0	0.67	8.01	…

obtain an estimate of the temperature dependent diffusion coefficient for Nd in liquid Mg derived from the Eqs. (1)–(3):

$$D \approx (C_s - C_z)\frac{dL}{dt}\frac{\delta}{C_i} \quad . \tag{4}$$

Substituting the values in Table IV into Eq. (4) gives $D_{725} = 4.38 \times 10^{-8}$ cm^2/s. The same method can be used to solve for the diffusion coefficient at the other temperatures. For the other calculations, it was assumed that C_S, C_Z, C_i, and δ remained relatively constant. This assumption is believed to be fairly accurate for the following reasons. First, the convection currents in the molten Mg which determine C_i and δ are expected to be sufficiently rapid for all the experimental conditions used to cause similar values for C_i and δ. Second, the contrast of the diffusion layers using BSE for all the samples was essentially identical, indicating that C_Z is fairly constant. Thus, only the changes in T, t, and L need to be considered to calculate the diffusion coefficient. Following the same procedure as for the 725 °C data, the calculated diffusion coefficients for the other temperatures are listed in Table V. Note that the calculated diffusion coefficients are the same no matter whether the measured Nd composition or the adjusted Nd composition is used. This is because the Nd composition used in Eq. (4) is based on the relative changes in composition rather than absolute values. As expected, the diffusion coefficient increases from 675 to 750 °C.

TABLE V. Calculated values of diffusion coefficient of Nd in liquid Mg, D.

Casting temperature	Calculated average diffusion coefficient D (cm^2/s)
948 K (675 °C)	$4.20 \times 10^{-10} \pm 1.86 \times 10^{-10}$
973 K (700 °C)	$4.61 \times 10^{-8} \pm 1.34 \times 10^{-8}$
998 K (725 °C)	$4.78 \times 10^{-8} \pm 1.56 \times 10^{-8}$
1023 K (750 °C)	$8.98 \times 10^{-8} \pm 3.50 \times 10^{-8}$

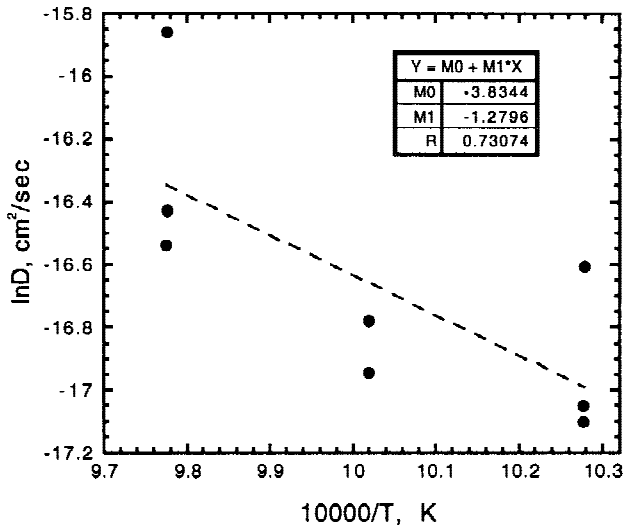

FIG. 11. Plot of ln D versus $1/T$.

It is known the diffusion coefficient is a function of temperature and can be represented by an Arrhenius relationship of the form[23]

$$D = D_0 e^{-Q/RT} \tag{5}$$

A rough estimate of the temperature independent constant D_0 and the activation energy Q can be made by plotting ln D versus $1/T$ which gives D_0 as the y-intercept and $-Q/R$ as the slope. Since only one data point was obtained at 675 °C, that point was omitted from subsequent analysis. This is shown in Fig. 11. Obtaining a best fit line to the 700, 725, and 750 °C data allows the values for D_0 and Q to be calculated using standard methods. Doing this gives D_0 and Q as 2.16×10^{-2} cm^2/s and 1.06×10^2 kJ/mol, respectively.

V. SUMMARY AND CONCLUSIONS

(1) Using molten magnesium to remove Nd from NdFeB magnet scrap and particulate with size range from 20 to 50 mesh by diffusion is an effective method of recovering Nd from waste byproducts of rare earth magnet manufacture. Diffusion proceeds rapidly at temperatures above 700 °C, enriching the Mg with Nd.

(2) The molten Mg matrix consists of two phases upon solidification: a binary eutectic consisting of solid solution α–Mg + Nd and $Mg_{12}Nd$. The $Mg_{12}Nd$ is present in two forms, intergranularly and as Widmanstatten plates within the grains.

(3) From the Nd composition profile across the diffusion layer, a two-phase zone forms which contains very little Nd. If one assumes that the average composition of Nd in the two-phase zone remains constant at C_Z, and the thickness of the boundary layer in liquid Mg at the solid/liquid interface δ remains constant during the casting process, the mass transport process of Nd through NdFeB scrap can be explained.

(4) If one lets the flux of Nd out of the scrap equal the flux into the liquid Mg, the diffusion coefficient of Nd in liquid Mg can be calculated. Doing this gives diffusion coefficients of Nd in liquid Mg larger than 4.61×10^{-8} cm^2/s at temperatures above 700 °C. The temperature-independent constant D_0 and the activation energy Q can be estimated as 2.16×10^{-2} cm^2/s and 1.06×10^2 kJ/mol, respectively, for Nd in liquid Mg.

ACKNOWLEDGMENTS

The authors acknowledge the work of L. Lincoln and C. Gross of the Ames Laboratory Materials Preparation Center for preparing and analyzing the materials used in

this study. The guidance of J. Verhoeven, F. Schmidt and T.W. Ellis is especially appreciated, along with helpful discussions with Alan Russell. This work was partially funded by a Carver Trust grant from ISU and was performed at Ames Laboratory, operated for the United States Department of Energy by Iowa State University under Contract No. W-7504-Eng82.

REFERENCES

1. J.W. Morrison and G.R. Palmer, Second International Symposium, Recycling of Metals and Engineered Materials, Williamsburg, VA 28–31, pp. 593–609 (Oct. 1990).
2. J.W. Lyman and G.R. Palmer, High Temp. Mater. Processes (London) **11**(1–4), 175–187 (1993).
3. B. Greenberg, Neodymium Recovery Process, U.S. Patent No. 5 362 459 (Nov. 8, 1994).
4. D.T. Peterson and R. Kontrimas, J. Phys. Chem. **64,** 362 (1960).
5. T.W. Ellis, F.A. Schmidt, and L.L. Jones, *Metals and Materials Waste Reduction, Recovery and Remediation* (The Minerals, Metals & Materials Society, Warrendale, PA, 1994), pp. 199–206.
6. I. Yu Mukhina, V.M. Lebedev, Kyung-Hyun Kim, and In-Bae Kim, J. Adv. Mater. **3,** 362 (1996).
7. Discussion with Ken Clark, then at Fansteel-Wellman Dynamics, of Creston, IA.
8. W. Zhang, G. Liu, and K. Han, J. Phase Equilib. **13,** (1992).
9. Joachim Wecker, Z. Metallkd. **81,** 157 (1990).
10. P. Villars, A. Prince, and H. Okamoto, *Handbook of Ternary Alloy Phase Diagram* (ASM, Materials Park, OH, 1995), Vol. 5, p. 5599.
11. *Binary Alloy Diagram,* edited by T.B. Massalski (American Society for Metals, Materials Park, OH, 1986), Vol. 1, p. 1085.
12. P.G. Shewmon, *Diffusion in Solids* (TMS, Warrendale, PA, 1989), pp. 131–148.
13. G.H. Geiger and D.R. Poirier, *Transport Phenomena in Metallurgy* (Addison-Wesley, Reading, MA, 1980). p. 431.